Palaeogeography, Palaeoclimatology, Palaeoecology 654 (2024) 112418

Contents lists available at ScienceDirect

Palaeogeography, Palaeoclimatology, Palaeoecology

journal homepage: www.elsevier.com/locate/palaeo

Elevated sea surface temperature and enhanced primary productivity during Ocean Anoxic Event 1d in the eastern Tethys: Calcareous nannofossil evidence from southern Tibet, China

Yasu Wang [a], Shijun Jiang [a,b,*], Ying Cui [c], Ruize Liang [a], Hong Su [d]

[a] College of Oceanography, Hohai University, Nanjing 210024, China
[b] Southern Marine Science and Engineering Guangdong Laboratory (Zhuhai), Zhuhai 519080, China
[c] Department of Earth and Environmental Studies, Montclair State University, Montclair, NJ 07043, USA
[d] College of Life Science and Technology, Jinan University, Guangzhou 510632, China

ARTICLE INFO

Editor: Z Han

Keywords:
Calcareous nannofossil
Biostratigraphy
Nutrient index
Temperature index
Ocean Anoxic Event 1d (OAE 1d)
Southern Tibet

ABSTRACT

Mid-Cretaceous oceanic anoxic events (OAEs) are characterized by major disturbances to the global carbon cycle and are considered ancient analogs for anthropogenic global warming. Among these events, OAE 1d, occurring around the Albian-Cenomanian boundary, remains understudied in the eastern Tethys region, leaving a critical palaeogeographic gap that hampers a global understanding of its impacts. In this paper, we present a detailed record of calcareous nannofossil assemblages from the lower to middle part of the Lengqingre Formation in the Chaqiela section of Gamba, southern Tibet, China. The study interval contains abundant, moderately to well preserved calcareous nannofossil assemblages, with *Watznaueria barnesiae*, *Discorhabdus ignotus*, *Biscutum constans*, and *Zeugrhabdotus erectus* as the dominant species constituting >50% of the assemblages. These nannofossil assemblages allow the study interval to be constrained to Upper Cretaceous (UC) Biozones UC0 through UC2, with the Albian-Cenomanian boundary located in the lower part of the Lengqingre Formation, and the middle part assigned to Cenomanian in the study area. As such, the position of OAE 1d in this section is accurately determined. Calculated nutrient and temperature indices based on nannofossil species with preferred ecologies reveal significant palaeoceanographic changes across the OAE 1d. These changes show increased abundance of warm-water taxa (*e.g.*, *Rhagodiscus asper* and *Zeugrhabdotus diplogrammus*) and high-productivity taxa (*e.g.*, *D. ignotus*, *B. constans*, and *Z. erectus*), suggesting increased sea surface temperature and enhanced productivity during OAE 1d in the southwestern shelf sea of the eastern Tethys Ocean.

1. Introduction

The Mid-Cretaceous witnessed a series of significant oceanic anoxic events (OAEs) that profoundly impacted Earth's climatic and palaeoceanographic history, representing major disturbances to the global carbon cycle (Schlanger and Jenkyns, 1976; Jenkyns, 2010; Bottini and Erba, 2018; Kabanov et al., 2023). Among these events, OAE 1d stands out as a pivotal episode occurring close to the boundary between the Albian and Cenomanian stages (Jenkyns, 2010). These OAEs serve as crucial analogues for unraveling the mechanisms causing these events and understanding their profound implications for anthropogenic carbon cycle perturbation (Richey et al., 2018).

OAEs play a critical role in shaping marine ecosystems and climate dynamics. Currently available data suggest that the major triggering mechanisms behind these short-lived events were abrupt rise in temperature, induced by rapid influxes of CO_2 into the atmosphere from volcanogenic and/or methanogenic sources (Schlanger and Jenkyns, 1976; Hesselbo et al., 2000; Wagreich et al., 2011; Yao et al., 2021). The resulting global warming led to widespread oceanic oxygen depletion, an accelerated hydrological cycle, increased continental weathering, and enhanced nutrient discharge to waterbodies. Consequently, there was heightened organic carbon production and burial, which left black shale as key sedimentary signature and carbon isotope excursions as geochemical fingerprints (Schlanger and Jenkyns, 1976; Jenkyns, 2010; Richey et al., 2018; Reershemius and Planavsky, 2021).

Despite a wealth of studies focused on OAEs, current research on OAE 1d is primarily concentrated in the western Tethys and North Atlantic regions (e.g., Herrle et al., 2003; Erba, 2004; Bottini and Erba,

* Corresponding author at: College of Oceanography, Hohai University, Nanjing 210024, China.
E-mail address: ssj0047@my.fsu.edu (S. Jiang).

https://doi.org/10.1016/j.palaeo.2024.112418
Received 31 December 2023; Received in revised form 23 July 2024; Accepted 28 July 2024
Available online 17 August 2024

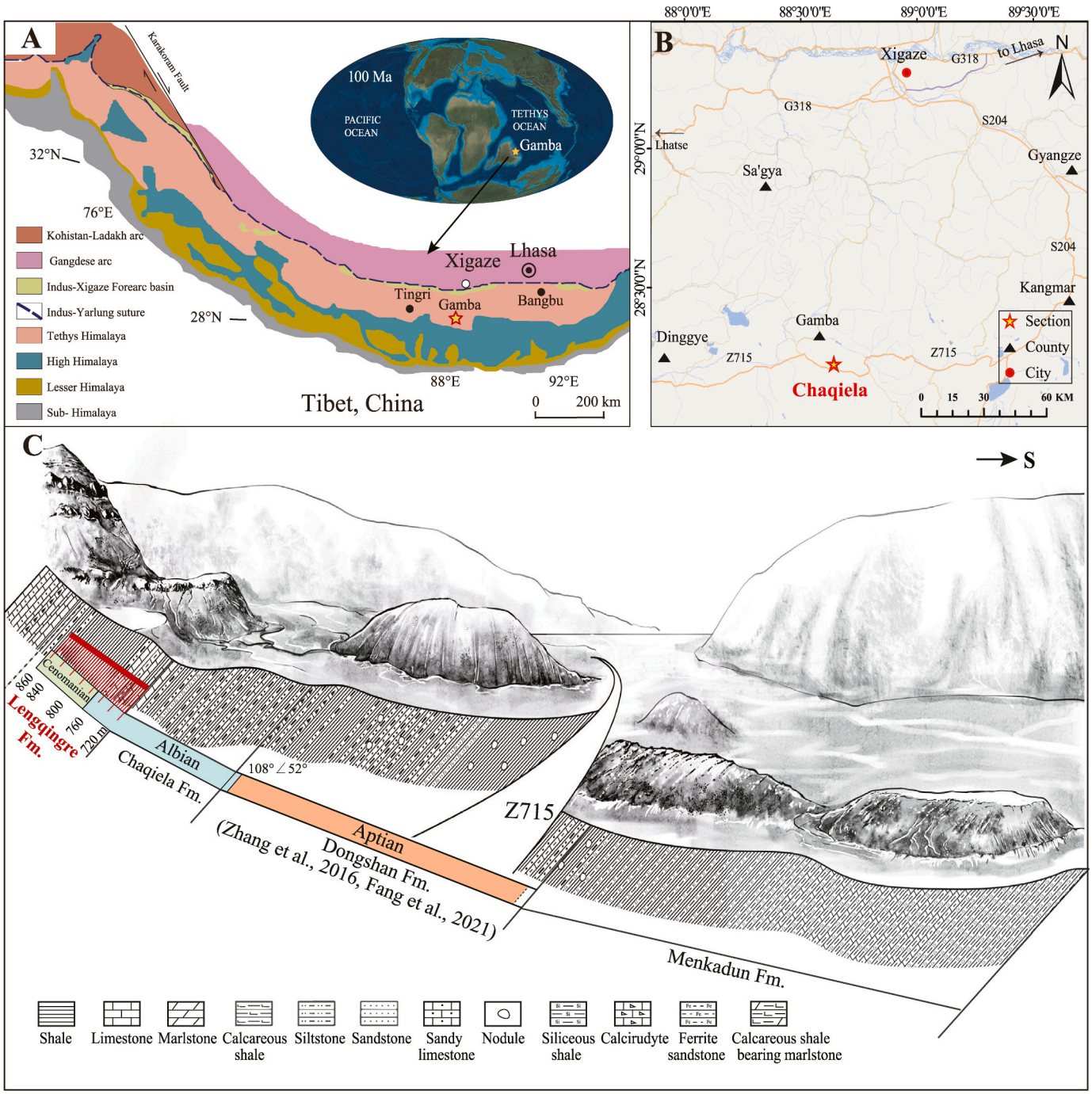

Fig. 1. (A) Global palaeogeographic map of the Late Cretaceous (~100 Ma) (modified from Blakey and Ranney, 2018) with a simplified geological map of the Himalaya and southern Tibet showing the locations of the study section and other sections mentioned in this study (modified from Hu et al., 2017); (B) Geographic location of the study section; (C) A sketch of the Chaqiela section showing the main lithologic units and the studied interval. Note that Fang et al. (2021) studied the planktonic foraminifera from the Dongshan Fm. (originally Gambadongshan Fm.), and the carbon isotope stratigraphy of Zhang et al. (2016) covered the interval from the Dongshan to the Lengqingre Fm. (lower part of their Gambacunkou Fm.). See the main text and Wan et al. (2000) for the updated definitions of these formations.

2018). Detailed examinations are limited in the eastern Tethys due to the short duration and relatively mild nature of this event, as well as sparse biostratigraphic constraints (Zhang et al., 2016; Yao et al., 2018; Yao et al., 2021). This geographic gap highlights a critical need for extensive and detailed investigation of the event in this region to obtain a holistic understanding of its mechanisms, impacts, and implications from a global palaeoceanographic perspective.

Precise timing is crucial for locating the stratigraphic position and exploring the nature and mechanisms of major geological events, and calcareous nannofossils serve as reliable geochronological markers. Their high abundance, robust preservation, and rapid evolution make them indispensable for constructing accurate geochronological frameworks (Perch-Nielsen, 1985; Bown, 1998; Erba, 2004), which has been shown to be particularly useful in the marine strata in Tibet (e.g., Xu and Mao, 1992; Zhong et al., 2000; Svabenicka et al., 2010; Hoshina et al., 2021; Wang et al., 2022; Zhang et al., 2023). Moreover, calcareous phytoplankton, a key group at the base of the Cretaceous marine ecosystem, have proven sensitive to environmental perturbations

associated with OAEs (Erba, 2004; Bottini and Erba, 2018). Yet, their response to OAE 1d in the eastern Tethys remains poorly known.

This study focuses on the Gamba region in southern Tibet (eastern Tethys; Fig. 1), which is known for its well-exposed and continuous Cretaceous marine sequences and represents an ideal location for investigating OAE 1d. Our main objectives are to: (1) identify OAE 1d through calcareous nannofossil biostratigraphy, (2) assess the variations in primary productivity through analysis of the calcareous phytoplankton assemblages, and (3) discern local *versus* basin-scale signals of OAE 1d through cross-ocean comparison. This research bridges a critical geographic gap in our understanding of marine productivity and environmental changes during OAE 1d in the surface shelf sea of southwestern Tethys.

2. Geological background

Southern Tibet, located in the eastern Tethys realm as the northern margin of the Indian plate during the Cretaceous (Fig. 1A), is divided from south to north into five tectonic belts: the High Himalayan Crystalline Belts, the Tethys Himalaya tectonic zone, the Indus-Yarlung Zangbo Suture Zone, the Xigaze forearc basin, and the Gandese Arc (Wang et al., 1996; Yin and Harrison, 2000). The Tethys Himalaya exhibits the most comprehensive and representative Cretaceous marine strata in China and is further subdivided into the southern and northern Tethys Himalaya by the Gyrong-Kangmar Thrust (GKT) (Ratschbacher et al., 1994) or Tingri-Gamba Thrust (TGT) (Tapponnier et al., 1981; Wang et al., 2005). The northern Tethys Himalaya mainly consists of continental slope to pelagic basin deposits (Liu and Einsele, 1994; Li et al., 2005; Hu et al., 2008), while the southern Tethys Himalaya is dominated by shallow shelf sedimentary rocks or slope deposits (Liu and Einsele, 1994; Willems et al., 1996). The studied section, Chaqiela section, lies in the Gamba area in the southern Tethyan Himalaya (Fig. 1A).

Intensive research has been conducted on the Cretaceous strata in the Gamba and nearby Tingri areas, Southern Tibet (Wen, 1974; Wang et al., 1980; Wan, 1985; Xu and Mao, 1992; Willems et al., 1996; Zhang et al., 2012; Hu et al., 2017; Fang et al., 2021; Li et al., 2022; Wang et al., 2022; Zhang et al., 2023), making it an ideal area for investigating the evolution of the eastern Tethys, the India-Asia continental collision, and major oceanic events. Based on lithostratigraphic and biostratigraphic studies in the Gamba area according to Wan et al. (2000), the Cretaceous sedimentary succession is divided into five formations from bottom to top: Dongshan Formation (Fm.), Chaqiela Fm., Lengqingre Fm., Gambacunkou Fm., and Zongshan Fm., with the Albian/Cenomanian (~100.5 Ma) identified between the Chaqiela and Lengqingre Fm. in the Gamba area. It is important to note the inconsistency among researchers regarding the definitions of the Chaqiela and Gambacunkou Fm. (including the subsequently divided Lengqingre, Xiawuchubo, and Jiubao Fm.) in the Gamba area (see Wan et al., 2000 for a detailed review). In this study, we followed the definitions of these formations as outlined by Wan et al. (2000). The organic-rich black shales in the Lengqingre Fm. are considered an expression of mid-Cretaceous oceanic anoxic events, making them crucial for global correlation.

The Chaqiela section (28°14′3.05″, 88°37′53.60″) studied here belongs to the Southern Tethyan Himalaya. It is located ~12 km east of Gamba County and outcrops to the north of the Z715 road (Fig. 1B), a newly paved county road with an asphalt surface providing easy access to the section. The sedimentary succession is approximately 643 m thick and mainly composed of black to gray shales with a greenish gray weathering color, and includes many interbeds of argillaceous limestones and sandstones (Fig. 1C) (Wan et al., 2000; Li et al., 2016).

3. Materials and methods

3.1. Calcareous nannofossil analyses

A total of 99 samples was collected at ~5 m intervals from the Chaqiela Fm., and 56 samples were taken at ~2.5 m (equivelent to real thicness) intervals from the middle-lower part of the Lengqingre Fm. in the Chaqiela section during a field trip in 2021. To obtain fresh materials and avoid weathering contamination during sampling, large rock pieces were knocked off outcrops with a hammer, and only those without cracks were selected and shaved to remove weathered surface. The 99 samples from the Chaqiela Fm. (0–708 m) are nearly barren of calcareous nannofossils. Therefore, the 56 samples from the middle-lower part of the Lengqingre Fm. were prepared as smear slides and examined to determine biostratigraphic ranges, preservation, and abundance of calcareous nannofossils. The preparation of smear slides for calcareous nannofossil analysis followed the modified "double slurry" method (Watkins and Bergen, 2003; Jiang and Zhang, 2016), mounted with Norland optical adhesive No. 61 and cured under UV light. This method allows better fossil dispersion and assemblage representation from coarse clastic sediments when large sample sizes are needed. All of the slides were examined with a Zeiss Axio Imager.A2 light microscope under crossed-polarized and plane-transmitted light at 1000× magnification. Micrographs were taken with a Zeiss Axiocam 506 color 6-megapixel digital camera.

The overall preservational state of calcareous nannofossils in each slide was evaluated by visual estimation to assess specimen dissolution and/or overgrowth based on the three-catergory criteria proposed by Watkins (1992). The quantitative analysis of each slide was conducted based on the following criteria: (1) three randomly selected traverses (1 traverse = 40 mm, ~100 fields of view) were browsed for each slide; (2) all specimens were counted from at least 15 randomly selected fields of view (FOVs) with materials evenly dispersed; (3) the minimum count was 400 specimens; and (4) for samples with very rare nannofossils, all specimens in three random transverses were counted. Additionally, three more traverses were scanned to increase the chance of observing those rare but stratigraphically important marker species. If found, these were not added to the total counts but indicated on the distribution chart by 'P'. Relative abundance, as the percentage of each taxon, was calculated except for samples with total specimen counts <100. Species richness, the number of different species represented in a calcareous nannofossil assemblage, was used to estimate community diversity. The total abundance of calcareous nannofossil assemblages was estimated as the number of specimens normalized to 100 FOVs.

Calcareous nannofossil taxonomy was determined following the classic concepts (Perch-Nielsen, 1985; Bown, 1998), which are mostly included and updated in the Nannotax3 online database (Young et al., 2017; http://www.mikrotax.org/Nannotax3/). Both the NC biozonation scheme of Roth (1978) and UC zones of Burnett et al. (1998) were used for the biostratigraphic study, and biostratigraphy was based on the first occurrence (FO) and last occurrence (LO) of marker species, which were given orbitally-tuned ages according to Gradstein et al. (2004). According to Roth (1978) and Bralower et al. (1995), the nannofossil Subzone NC10a ranges from the FO of *Eiffellithus turriseiffelii* (103.13 Ma) to the FO of *Corollithion kennedyi* (100.45 Ma), and NC10b from the FO of *Corollithion kennedyi* to the LO of *Lithraphidites acutus* (94.39 Ma). Correspondingly, the UC0 zone ranges from the FO of *Eiffellithus turriseiffelii* to the LO of *Hayesites aibiensis* (100.84 Ma), the UC1 zone from the FO of *C. kennedyi* to the FO of *Gartnerago segmentatum* (98.26 Ma), and the UC2 zone from the FO of *G. segmentatum* to the FO of *L. acutus*. When a zonal marker occurred sporadically, the bioevents were identified based on the intervals where the marker was well preserved and continuously present.

3.2. Calculation of palaeoenvironmental indice

Nannofossil preservational state was quantitatively assessed by the whole shield index (WSI) proposed by Bralower et al. (2018). This index is calculated by determining the ratio of complete *W. barnesiae* specimens to the sum of complete and broken specimens, with higher values indicating better preservation. Nutrient index (NI) and temperature

Fig. 2. Distribution chart of calcareous nannofossils from the middle-lower part of the Lengqingre Fm. in the Chaqiela section, Gamba area, southern Tibet. Note: C = common (1 specimen per 2–10 FOVs), F = few (1 specimen per 11–100 FOVs), and R = rare (1 specimen per 101–1000 FOVs). The red lines represent the distribution of key zonal markers. (For interpretation of the references to color in this figure legend, the reader is referred to the web version of this article.)

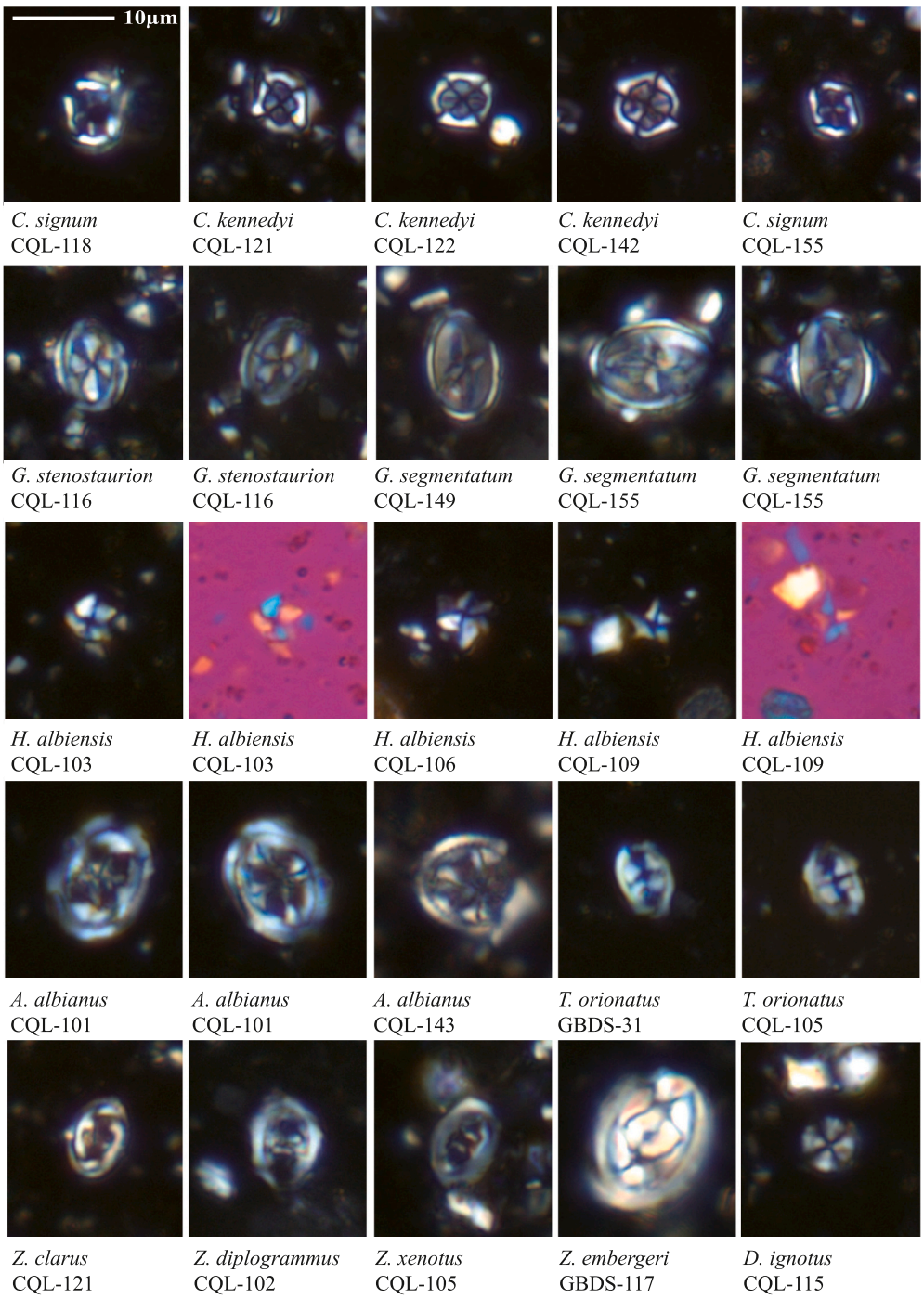

Fig. 3. Selected calcareous nannofossils of the Lengqingre Fm. from the Chaqiela section, Gamba area, southern Tibet (scale bar applies to all micrographs). 1–*Corollithion signum*; Sample CQL- 118. 2, 3, 4–*Corollithion kennedyi*; Sample CQL-121; CQL-122; CQL-142. 5–*Corollithion signum*; Sample CQL-155. 6, 7–*Gartnerago stenostaurion*; Sample CQL-116. 8, 9, 10–*Gartnerago segmentatum*; Sample CQL-149; CQL-155. 11–15–*Hayesites albiensis*; Sample CQL-103; CQL-106; CQL-109. 16–18–*Axopodorhabdus albianus*; Sample CQL-103; CQL-143. 19,20–*Tranolithus orionatus*; Sample GBDS- 31; CQL-105. 21–*Zeugrhabdotus clarus*; Sample CQL-121. 22–*Zeugrhabdotus diplogrammus*; Sample CQL-102. 23–*Zeugrhabdotus xenotus*; Sample CQL-105. 24–*Zeugrhabdotus embergeri*; Sample CQL-117. 25–*Discorhabdus ignotus*; Sample CQL-115.

index (TI) were calculated following the methods of Herrle (2003), Watkins et al. (2005), and Bottini et al. (2015), and the modification of Bottini and Erba (2018). There methods have been successfully applied to the mid-Cretaceous interval, with higher TI values indicating low temperatures and higher NI values indicating higher productivity.

Specifically, NI was calculated based on three high-productivity species (*Biscutum constans*, *Zeugrhabdotus erectus*, *Discorhabdus ignotus*) and a low-productivity species (*W. barnesiae*), and the ecologies of these taxa were based on numerous previous stidues on their palaeobiogeographic distribution and correlation with other geochemical proxies (e.g., Roth and Krumbach, 1986; Erba et al., 1992; Williams and Bralower, 1995; Herrle, 2003; Bornemann et al., 2005; Mutterlose et al., 2005; Tremolada et al., 2006; Tiraboschi et al., 2009). This index is defined as:

$$NI = \frac{\mathrm{Bi} + \mathrm{Zi} + \mathrm{Di}}{\mathrm{Bi} + \mathrm{Zi} + \mathrm{Di} + \mathrm{Wi}} \times 100$$

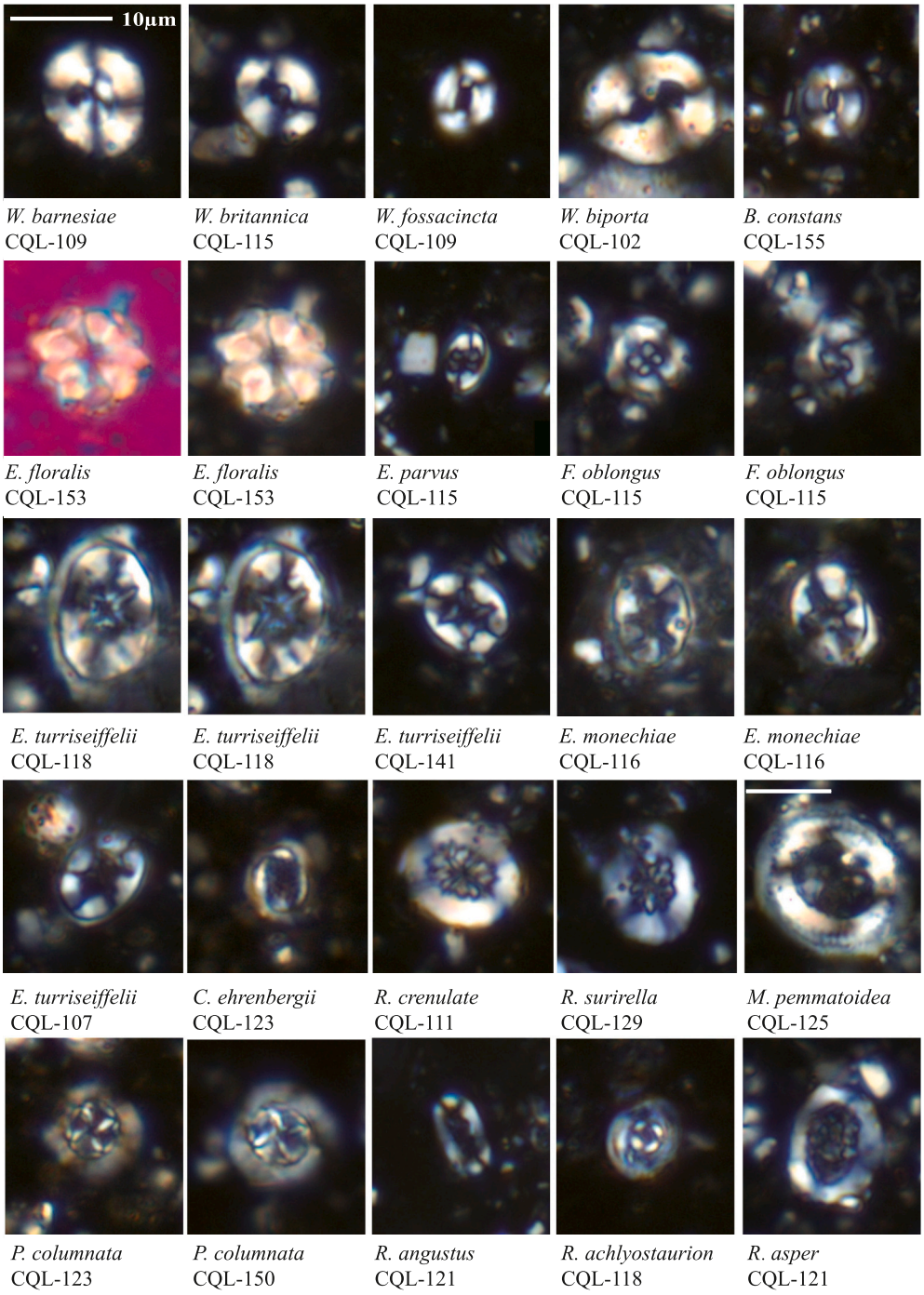

Fig. 4. Selected calcareous nannofossils of the Lengqingre Fm. from the Chaqiela section, Gamba area, southern Tibet (scale bar applies to all micrographs). 1–*Watznaueria barnesiae*; Sample CQL-109. 2–*Watznaueria britannica*; Sample CQL-115. 3–*Watznaueria fossacincta*; Sample CQL-109. 4–*Watznaueria biporta*; Sample CQL-102.5–*Biscutum constans*; Sample CQL-155. 6, 7–*Eprolithus floralis*; Sample CQL-153. 8–*Eiffellithus parvus*; Sample CQL-115. 9,10–*Flabellites oblongus*; Sample CQL-115. 11–13–*Eiffellithus turriseiffelii*; Sample CQL-118; CQL-141. 14,15–*Eiffellithus monechiae*; Sample CQL-116. 16–*Eiffellithus turriseiffelii*; Sample CQL-107. 17–*Cribrosphaerella ehrenbergii*; Sample CQL-123. 18–*Retecapsa crenulate*; Sample CQL-111. 19–*Retecapsa surirella*; Sample CQL-129. 20–*Manivitella pemmatoidea*; Sample CQL- 125. 21,22–*Prediscosphaera columnata*; Sample CQL-123; CQL-150. 23–*Rhagodiscus angustus*; Sample CQL-121. 24–*Rhagodiscus achlyostaurion*; Sample 118. 25–*Rhagodiscus asper*; Sample CQL-121.

where Bi = *Biscutum constans*, Zi = *Zeugrhabdotus erectus*, Di = *Discorhabdus ignotus*, and Wi = *Watznaueria barnesiae*, each expressed as a percentage.

TI was calculated based on two warm-temperature species (*Rhagodiscus asper*, *Zeugrhabdotus diplogrammus*) and three cool-temperature species (*Staurolithites stradneri*, *Eprolithus floralis*, *Repagulum parvidentatum*) based on previous paleceogical studies (*e.g.*, Roth and Krumbach, 1986; Bralower, 1988; Wise, 1988; Erba et al., 1992; Herrle and Mutterlose, 2003; Herrle et al., 2003; Tiraboschi et al., 2009). Due to the absence of typical *Repagulum parvidentatum* in the study sequence possibly due to environmental exclusion in the eastern Tethys (Zhang et al., 2023), the formula for TI was modifed to:

$$TI = \frac{\mathrm{Si} + \mathrm{Ei}}{\mathrm{Si} + \mathrm{Ei} + \mathrm{Ri} + \mathrm{Zi}} \times 100$$

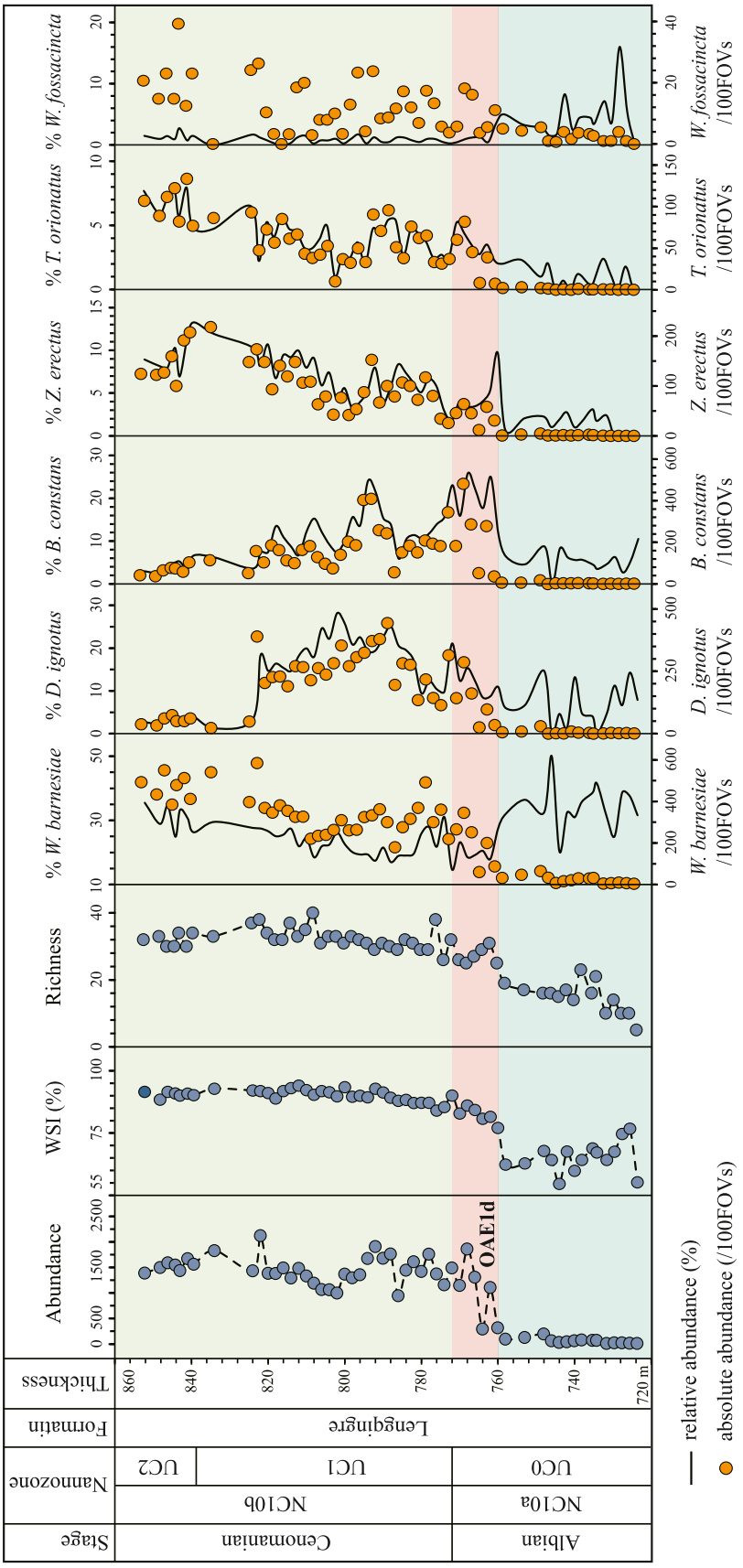

Fig. 5. Variations in abundance, whole shield index (WSI), species richness, and main calcareous nannofossil species across the OAE 1d in the Chaqiela section, Gamba, southern Tibet. The solid lines denote percentage abundance, and the filled circles indicate absolute abundance (number of specimens encountered in 100 FOVs).

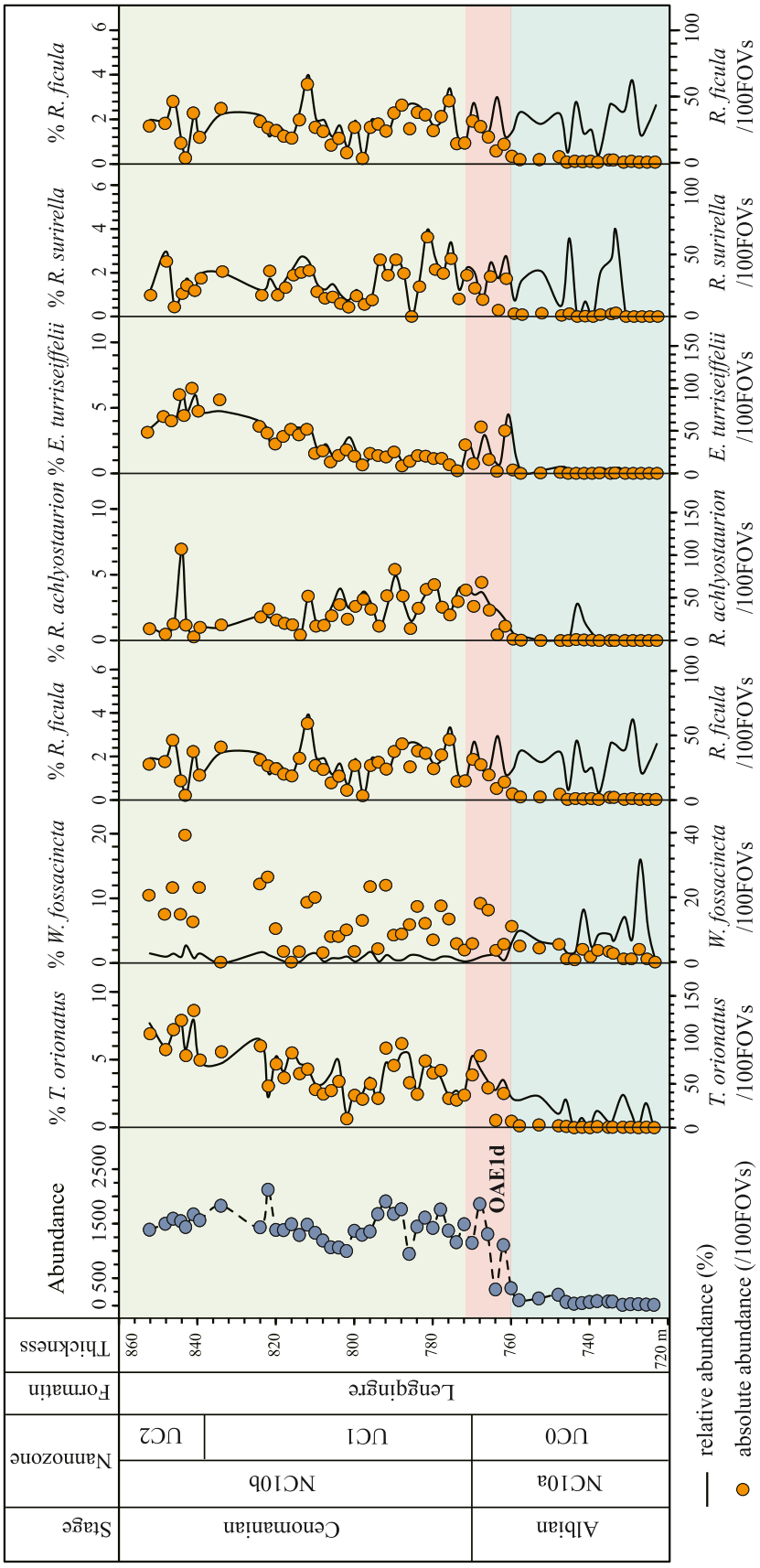

Fig. 6. Variations in main calcareous nannofossil species across the OAE 1d at the Chaqiela section, Gamba, southern Tibet. The solid lines denote percentage abundance, and the filled circles indicate absolute abundance (number of specimens encountered in 100 FOVs).

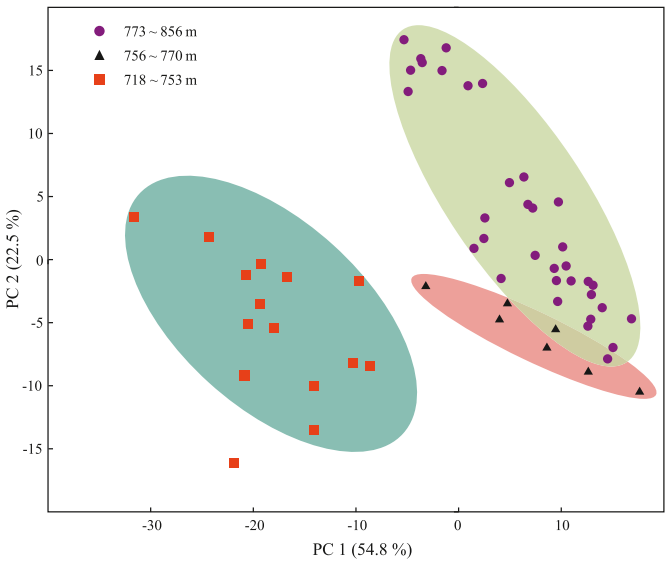

Fig. 7. Results of Principal Component Analysis. Note the distinct separation of the samples from the pre-OAE 1d, OAE 1d, and post-OAE 1d intervals.

where Si = *Staurolithites stradneri*, Ei = *Eprolithus floralis*, Ri = *Rhagodiscus asper*, and Zi = *Zeugrhabdotus diplogrammus*, each expressed as a percentage.

To further explore the temporal variations in nannofossil assemblage and palaeoecology, Principal Component Analysis (PCA) was performed based on a variance-covariance matrix. The PCA analysis included all taxa at genus level using the free statistical software Past v4.06 (Hammer et al., 2001).

All slides are archived and deposited at College of Oceanography, Hohai University, Nanjing, China, and related data can be found in the Supplementary Data.

4. Results

Except for the five barren or near-barren samples from the lowermost part of our study interval in the Chaqiela section, all other samples yielded common to abundant, moderately to well preserved calcareous nannofossil assemblages. Overall, 74 species from 33 genera were identified, despite minor overgrowth with secondary calcite or slight etching by dissolution (Figs. 2, 3, 4; Supplementary Table S1). *Watznaueria barnesiae*, *Discorhabdus ignotus*, *Biscutum constans*, and *Zeugrhabdotus erectus* is predominant throughout the section and their abundances range between 14.6% to 50%, 0 to 28.2%, 0 to 25.9%, 0 to 13.3%, with averages of 26.7%, 12.2%, 10.2%, and 5.5%, respectively. Other common taxa include *Tranolithus orionatus*, *Watznaueria fossacincta*, *Retecapsa ficula*, and *Rhagodiscus achlyostaurion* (see Fig. 2 and Table S1 for a full list of taxa). Except for the two samples from the lowermost part of our study interval, the abundance of *W. barnesiae* does not exceed 40%.

Nannofossil Zone NC10, ranging from the FO of *Eiffellithus turriseiffelii* to the LO of *Lithraphidites acutus*, can be further subdivided into two subzones (NC10a and NC10b) by the FO of *Corollithion kennedyi* (770 m). Additionally, *Hayesites albiensis* is a zonal marker within Subzone NC10a, and its LO (100.84 Ma) was observed at 748 m. Therefore, interval 718–768 m can be assigned to the Subzone NC10a. The stratigraphically younger marker *Gartnerago segmentatum* was found, and its FO (98.26 Ma) observed at 838 m further defined interval 770–856 m as the Subzone NC10b. Based on the UC zones of Burnett et al. (1998), the FO of *Corollithion kennedyi* (770 m) is the zonal boundary between Zones UC0 and UC1, and the FO of *G. segmentatum* (838 m) marks the zonal boundary between Zones UC1 and UC2. Therefore, a continuous sequence of nannofossil Zones UC0 through UC2 was recognized from the study interval.

The Albian/Cenomanian boundary falls within the upper part of the Zone UC0 (Burnett et al., 1998; Kennedy et al., 2000; Gale et al., 2011), and the main part of OAE 1d has been shown to lie in the upper Albian, within the upper part of the Zone UC0 (Erba, 2004; Bottini and Erba, 2018). We identify the OAE 1d record based on presence of calcareous nannofossil Zone UC0 in the 756–768 m interval, thereby subdividing the study section into three intervals. The underlying pre-OAE 1d interval (718–753 m) has lower WSI values than the upsection intervals. The relative abundance of the dissolution-resistant *W. barnesiae* shows a decreasing trend from the bottom to the top of the study section, with substantially higher abundances above 756 m and an average of 34.3% (Fig. 5). The NI and TI have a mean value of 49.2 and 35.6, varying from 2 to 75.8 and 0 to 92.6, respectively (Fig. 6). In general, the NI values are among the highest within the OAE 1d interval, while the TI values are the lowest. There is a parallel variation trend between NI and PC1 (Fig. 7), which is relatively low in the pre-OAE 1d interval and subsequently increases upsection within the OAE 1d and post-OAE 1d intervals. This variation pattern holds true for the TI and PC2 values.

5. Discussion

5.1. Calcareous nannofossils biostratigraphy and presence of the OAE 1d in the Chaqiela section

Diagenetic processes exert substantial influences on the preservation of calcareous nannofossil assemblages within marine sediments, thereby significantly impacting their utility as palaeoceanographic indicators (Roth and Krumbach, 1986; Bruno et al., 2020). Several studies have proposed that when the relative abundance of *Watznaueria barnesiae* exceed 40%, the assemblage composition would be skewed and depart from the original nannofossil assemblage, indicating a strong influence of diagenesis (*e.g.*, Roth and Bowdler, 1981; Thierstein and Roth, 1991; Williams and Bralower, 1995). In our study, only 2 out of 56 samples from the pre-OAE 1d interval have *W. barnesiae* abundance exceeding 40%, suggesting that the nannofossil assemblages in our study section are minimally affected by dissolution and/or diagenesis. This suggestion is consistent with the fact that the OAE 1d and post-OAE 1d intervals contain well preserved nannofossil assemblages, as quantitatively indicated by the substantially higher WSI values (Fig. 5). Additionally, dissolution-sensitive taxa (*e.g.*, *Discorhabdus ignotus* and *Biscutum constans*) are abundant in all samples, with average abundance of 12.2% and 10.2%, respectively. Therefore, the calcareous nannofossil assemblages studied preserve the original compositions of the phytoplankton community, establishing their reliability for high-confidence palaeoceanographic reconstructions.

Existing studies of the Chaqiela section include a chronological framework established by palynological assemblages (Li et al., 2016), and dating of the Dongshan and Chaqiela Fm. to upper Barremian–Aptian with planktonic foraminifera (Fig. 1; Fang et al., 2021), and dating of the Dongshan–Gambacunkou Fm. to Aptian–Santonian based on carbon isotope chemostratigraphic correlation and planktonic foraminifera biostratigraphic constraints (Fig. 1; Zhang et al., 2016). However, the overlying Lengqingre Fm. still lacks a refined age. According to our calcareous nannofossil biostratigraphy, the middle-lower part of this formation is constrained to upper Albian to Cenomanian. The FO of *C. kennedyi* (100.45 Ma), which marks the boundary between Subzones UC0 and UC1 (Bralower et al., 1995), is placed at 770 m based on its continuous occurrences. This suggests that the Albian/Cenomanian boundary lies at 770 m in the Chaqiela section. Other observations bracket this age assignment: (1) the LO of *H. albiensis* (100.84 Ma) within Zone UC0 is determined at 748 m, which lies below the Albian/Cenomanian boundary; and (2) all the sporadic occurrences of *Eiffellithus turriseiffelii* (FO: 103.13 Ma) are present above the boundary. The FO of stratigraphically younger marker *G. segmentatum* (98.26 Ma)

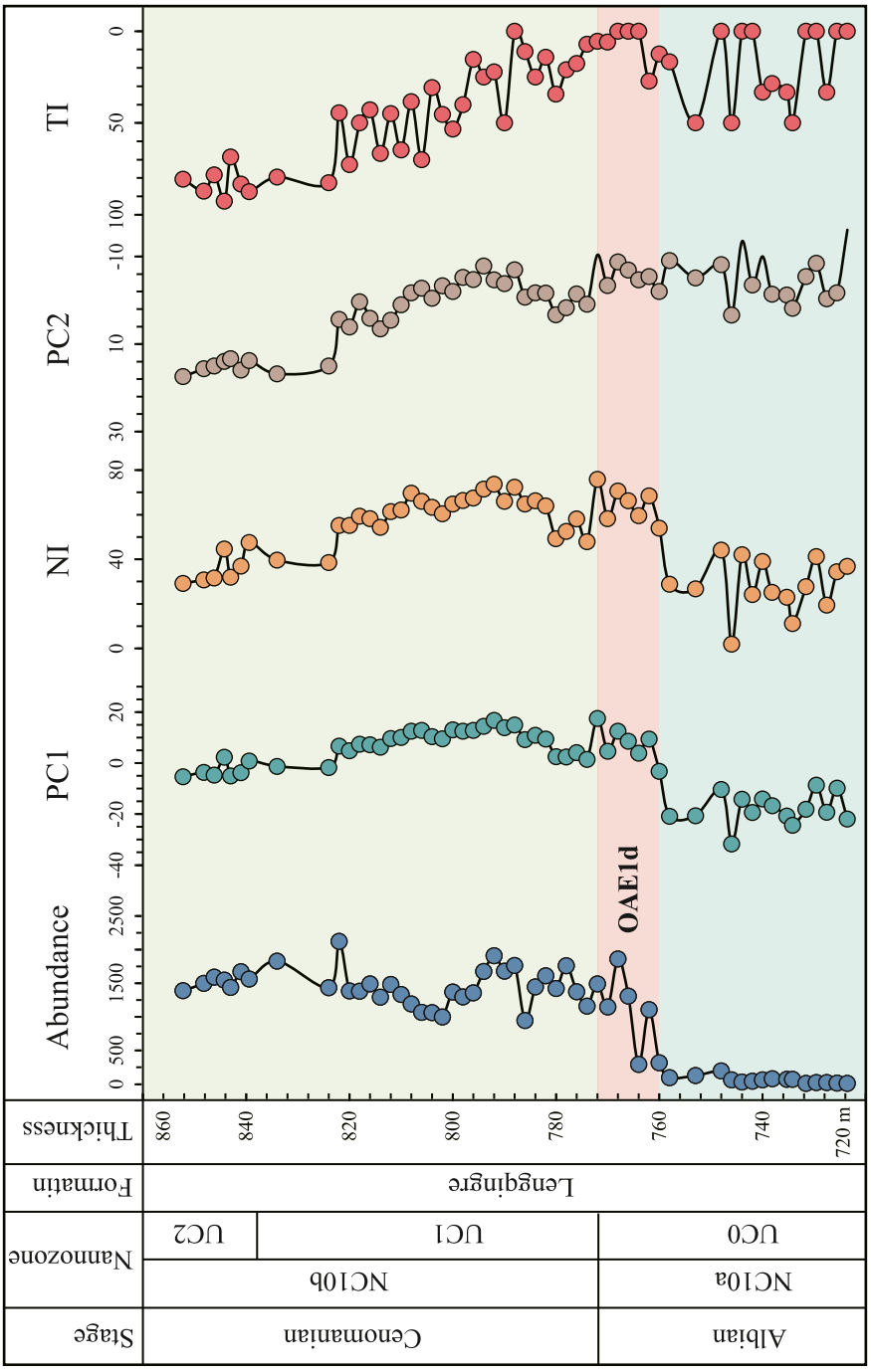

Fig. 8. Variations in abundance, PC1, nannofossil nutrient index (NI), PC2, and temperature index (TI). Because lower TI values indicate higher temperatures, the TI and PC2 values are plotted in reverse order for consistence with Fig. 7.

is determined at 838 m, further assigning interval 770–838 m to Zone UC1 and interval 838–856 m to Zone UC2. Therefore, a continuous sequence of nannofossil Zones UC0 through UC2 is established for the studied section. This helps mark the Albian/Cenomanian boundary (~100.5 Ma) at 770 m, within the lower part of the Lengqingre Fm., thereby dating its middle part to the Cenomanian in Gamba area. This finding is consistent with previous studies using planktonic foraminifera (Wan, 1985; Wan et al., 2003) and aligns with the results of Zhang et al. (2016) and Fang et al. (2021) from the perspective of stratigraphic superposition.

Geochronologically speaking, the main part of OAE 1d lies in the upper Albian, within the upper part of Zone UC0. Hence, we divide the study section into three intervals: the pre-OAE 1d interval (718–753 m), the OAE 1d interval (756–770 m), and the post-OAE 1d interval (773–856 m), and examine the assemblage changes and associated palaeoceanographic implications as follows.

5.2. *Variation in primary productivity in the southwestern surface shelf sea of the eastern Tethys Ocean across OAE 1d*

The OAE 1d event, known as the late Albian Breistroffer event, was initially identified in the Vocontian Trough of southeast France, resembling the lower Albian Niveau Paquier from a specific horizon (Bréhéret, 1994; Giraud et al., 2003; Bornemann et al., 2005). In addition to classic occurrences in the western Tethys (Bottini and Erba, 2018), this event has counterparts in the Northern Europe (Bąk et al.,

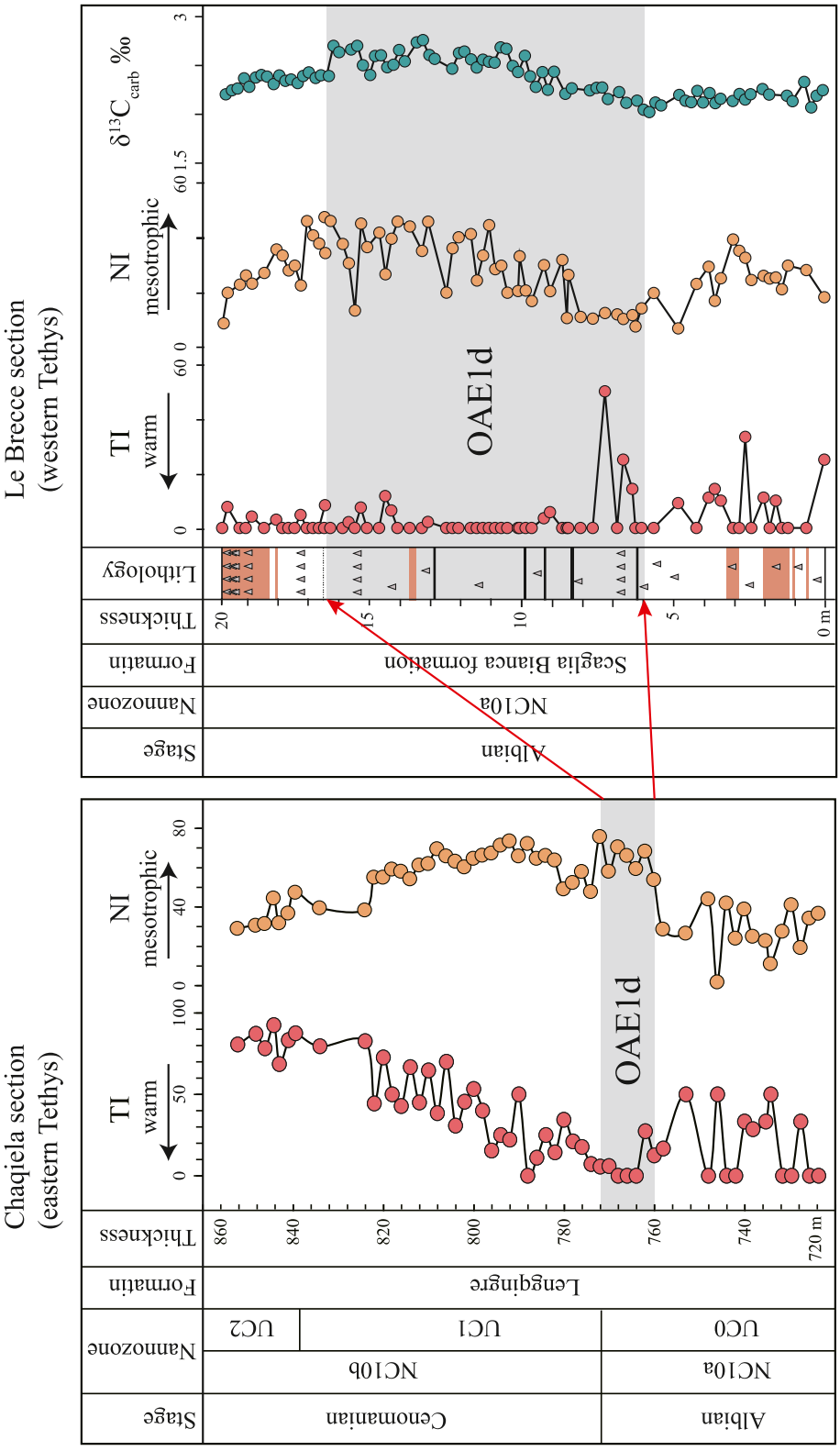

Fig. 9. Variations in nannofossil nutrient index (NI) and temperature index (TI) cross the OAE 1d in the Chaqiela section (Gamba area, China) and the classic Le Brecce section (Piobbico, Italy) (Gambacorta et al., 2015). Note the slightly thicker OAE 1d record at Chaqiela compared to Le Brecce (12 m *vs.* 10 m).

2016; Bornemann et al., 2017), the Pacific Ocean (Robinson et al., 2008), the Atlantic Ocean (Wilson and Norris, 2001; Watkins et al., 2005), the Southern Ocean (Fan et al., 2022), and in the US (*e.g.*, Grocke et al., 2006; Robinson et al., 2008; Richey et al., 2018), suggesting a global distribution (Barron, 1995; Wilson and Norris, 2001). Previous research has shown that OAE 1d represents an episode of enhanced productivity and organic carbon burial due to a collapse of the upper water column stratification (Wilson and Norris, 2001; Watkins et al., 2005). Below, we show how the calcareous nannoplankton, the major primary producers in the Cretaceous oceans that were sensitive to

changes in sea surface temperature (SST) and nutrient availability (Erba, 2004; Bottini and Erba, 2018), responded to the surface-water thermal structure change in the southwestern shelf sea of the eastern Tethys Ocean.

Several lines of evidence indicate that, during the pre-OAE 1d interval, the southwestern surface shelf sea of the eastern Tethys had lower nutrient availability and colder SST conditions. First, the abundance, species richness, and productivity indicator NI were low. *Discorhabdus ignotus*, *B.constans*, and *Z.erectus* are widely cited as indicators of elevated productivity based on numerous quantitative studies of assemblages from various mid-Cretaceous oceanic and epicontinental settings (*e.g.*, Erba et al., 1992; Herrle and Mutterlose, 2003; Watkins et al., 2005). The low abundances of these three high-productivity species are consistent with the higher proportions of low-productivity species *W. barnesiae* during pre-OAE 1d interval (Figs. 5, 6). Additionally, *Rhagodiscus asper* and *Zeugrhabdotus diplogrammus* are well-established warm-water taxa, while *Staurolithites stradneri* and *Eprolithus floralis* are cool-water taxa (*e.g.*, Roth and Krumbach, 1986; Bralower, 1988; Wise, 1988; Erba et al., 1992; Herrle and Mutterlose, 2003; Herrle et al., 2003; Tiraboschi et al., 2009). The high TI values and low NI values based on these taxa indicate that the pre-OAE 1d interval was a period of relatively low temperature and low productivity in the southwestern surface shelf sea of the eastern Tethys.

As OAE 1d event occurred, there was a rapid increase in total nannofossil abundance, species richness, and high-productivity indicators (*e.g.*, *D.ignotus*, *B.constans*, and *Z.erectus*), accompanied by a reduction in low-productivity indicator *W. barnesiae*. Additionally, there was a remarkable increase in warm-water species abundance and a decrease in cold-water species abundance (Figs. 5, 6). These observations support surface-ocean warming and increased productivity during OAE 1d, which is corroborated by significant changes in the NI and TI values. Warming can accelerate terrestrial weathering, supplying more nutrients to boost oceanic primary productivity (Fu et al., 2017; Them et al., 2017), leading to the formation of black shale in the sedimentary record. During the post-OAE 1d interval, temperature and nutrient gradually returned toward the pre-OAE 1d levels, as evidenced by the diminished total nannofossil abundance and NI values, and increased TI values.

The PCA results summarize the overall response of nannofossil assemblages to OAE 1d. Two principal components (PC1 and PC2) were extracted, explaining 54.8% and 22.5% of the total variance, respectively (Fig. 7), which show parallel variation with NI and TI (Fig. 8). The sample plot allows us to distinguish three well-separated groups, corresponding to the three intervals across OAE 1d. The wide separation of these three groups suggests that the nannofossil assemblages experienced fundamental changes, and the surface ocean did not fully recover to the pre-OAE 1d conditions (Fig. 7). These fundamental palaeoceanographic changes observed in the southwestern surface shelf sea of the easternTethys have previously been seen in the western Tethys (Fig. 9), further confirming the global nature of OAE 1d.

6. Conclusions

We examine the calcareous nannofossil assemblages from the middle-lower part of the Lengqingre Fm. in the Chaqiela section, located in southern Tibet within the eastern Tethys. The nannofossil assemblages are abundant and moderately to well-preserved, with *W. barnesiae*, *D. ignotus*, *B. constans*, and *Z. erectus* as the predominant species, jointly constituting >50% of the assemblages. Based on the FO of *C. kennedyi* (770 m), the LO of *H. albiensis* (748 m), and the FO of *G. segmentatum* (838 m), a continuous sequence of nannofossil Zones UC0 through UC2 of late Albian–early Cenomanian age was established for the study interval. This zonation helps mark the Albian/Cenomanian boundary at the lower part of the Lengqingre Fm., date its middle part to the Cenomanian, and constrain the presence of OAE 1d in this section. Calculated nannofossil nutrient and temperature indices indicate that, during OAE 1d, the abundance of warm-water taxa (*e.g.*, *Rhagodiscus asper* and *Zeugrhabdotus diplogrammus*) increased, accompanied by higher numbers of eutrophic taxa (*e.g.*, *D. ignotus*, *B. constans*, and *Z. erectus*). This suggests warmed surface ocean and enhanced productivity during OAE 1d in the surface shelf sea of southwestern Tethys.

CRediT authorship contribution statement

Yasu Wang: Writing – review & editing, Writing – original draft, Visualization, Methodology, Investigation, Funding acquisition, Formal analysis, Data curation, Conceptualization. **Shijun Jiang:** Writing – review & editing, Writing – original draft, Visualization, Validation, Supervision, Project administration, Methodology, Investigation, Funding acquisition, Formal analysis, Data curation, Conceptualization. **Ying Cui:** Writing – review & editing, Validation, Formal analysis. **Ruize Liang:** Writing – original draft, Visualization, Data curation. **Hong Su:** Writing – original draft, Methodology.

Declaration of competing interest

The authors declare the following financial interests/personal relationships which may be considered as potential competing interests:

Shijun Jiang reports financial support was provided by National Key R&D Program of China. Shijun Jiang reports financial support was provided by National Natural Science Foundation of China. Yasu Wang reports financial support was provided by China Postdoctoral Science Foundation. Shijun Jiang reports financial support was provided by Innovation Group Project of Southern Marine Science and Engineering Guangdong Laboratory (Zhuhai). If there are other authors, they declare that they have no known competing financial interests or personal relationships that could have appeared to influence the work reported in this paper.

Data availability

Related data are included in Supplementary Table S1

Acknowledgments

This research is financially supported by the National Key R&D Program of China (2022YFF0800800), and National Natural Science Foundation of China (grants 42372004 & 42488201), China Postdoctoral Science Foundation (2022M720990), Innovational Fund for Scientific and Technological Personnel of Hainan Province (KJRC2023B04), and the Innovation Group Project of Southern Marine Science and Engineering Guangdong Laboratory (Zhuhai) (No. SML2023SP239). This is a contribution to the UNESCO IGCP 739.

Appendix A. Supplementary data

Supplementary data to this article can be found online at https://doi.org/10.1016/j.palaeo.2024.112418.

References

Bąk, K., Fabiańska, M., Bąk, M., Misz-Kennan, M., Zielińska, M., Dulemba, P., Bryndal, T., Naglik, B., 2016. Organic matter in upper Albian marine sediments in the High-Tatric units, central western Carpathians related to Oceanic Anoxic Event 1d—Geochemistry, microfacies and palynology. Palaeogeogr. Palaeoclimatol. Palaeoecol. 454, 212–227.

Barron, E.J., 1995. Tropical Climate Stability and Implications for the Distribution of Life. Effects of Past Global Change on Life. National Academy Press Studies in Geophysics, Washington, DC, pp. 108–117.

Bornemann, A., Pross, J., Reichelt, K., Herrle, J.O., Hemleben, C., Mutterlose, J., 2005. Reconstruction of short-term palaeoceanographic changes during the formation of the Late Albian 'Niveau Breistroffer' black shales (Oceanic Anoxic Event 1d, SE France). J. Geol. Soc. Lond. 162, 623–639.

Blakey, R.C., Ranney, W.D., 2018. Ancient Landscapes of Western North America: A Geologic History with Paleogeographic Maps. Springer, pp. 104–105.

Bornemann, A., Erbacher, J., Heldt, M., Kollaske, T., Wilmsen, M., Luebke, N., Huck, S., Vollmar, N.M., Wonik, T., 2017. The Albian-Cenomanian transition and Oceanic Anoxic Event 1d-an example from the Boreal Realm. Sedimentology 64, 44–65.
Bottini, C., Erba, E., 2018. Mid-cretaceous paleoenvironmental changes in the western Tethys. Clim. Past 14, 1147–1163.
Bottini, C., Erba, E., Tiraboschi, D., Jenkyns, H.C., Schouten, S., Sinninghe Damsté, J.S., 2015. Climate variability and ocean fertility during the Aptian Stage. Clim. Past 11, 383–402.
Bown, P.R., 1998. Calcareous Nannofossil Biostratigraphy. Kluwer Academic, Chapman and Hall.
Bralower, T.J., 1988. Calcareous nannofossil biostratigraphy and assemblages of the Cenomanian-Turonian boundary interval: Implications for the origin and timing of oceanic anoxia. Paleoceanography 3, 275–316.
Bralower, T.J., Leckie, R.M., Sliter, W.V., Thierstein, H.R., 1995. An integrated Cretaceous microfossil biostratigraphy. In: Berggren, W.A., Kent, D.V., Aubry, M.-P., Hardenbol, J. (Eds.), Geochronology, Time Scales and Global Stratigraphic Correlation. Special Publication - Society for Sedimentary Geology, pp. 65–79.
Bralower, T.J., Kump, L.R., Self-Trail, J.M., Robinson, M.M., Lyons, S., Babila, T., Ballaron, E., Freeman, K.H., Hajek, E., Rush, W., Zachos, J.C., 2018. Evidence for shelf acidification during the onset of the Paleocene-Eocene thermal maximum. Paleoceanogr. Paleoclimatol. 33, 1408–1426.
Bréhéret, J.-G., 1994. The Mid-Cretaceous Organic-Rich Sediments from the Vocontian Zone of the French Southeast Basin. In: Mascle, A. (Ed.), Hydrocarbon and Petroleum Geology of France. Springer, Berlin Heidelberg, Berlin, Heidelberg, pp. 295–320.
Bruno, M.D.R., Fauth, G., Watkins, D.K., Savian, J.F., 2020. Albian–Cenomanian calcareous nannofossils from DSDP Site 364 (Kwanza Basin, Angola): Biostratigraphic and paleoceanographic implications for the South Atlantic. Cretac. Res. 109, 104377.
Burnett, J., Gallagher, L., Hampton, M., 1998. Upper cretaceous. In: Bown, P.R. (Ed.), Calcareous Nannofossil Biostratigraphy, pp. 132–199.
Erba, E., 2004. Calcareous nannofossils and Mesozoic oceanic anoxic events. Mar. Micropaleontol. 52, 85–106.
Erba, E., Castradori, D., Guasti, G., Ripepe, M., 1992. Calcareous nannofossils and Milankovitch cycles; the example of the Albian Gault Clay Formation (southern England). Palaeogeogr. Palaeoclimatol. Palaeoecol. 93, 47–69.
Fan, Q., Xu, Z., MacLeod, K.G., Brumsack, H.-J., Li, T., Chang, F., Wan, S., Riquier, L., Fu, D., Luan, Z., Duan, B., Chen, H., Wang, W., Lim, D., 2022. First record of Oceanic Anoxic Event 1d at Southern High Latitudes: sedimentary and geochemical evidence from international ocean discovery program expedition 369. Geophys. Res. Lett. 49, e2021GL097641.
Fang, P., Luo, H., Xu, B., Huber, B.T., Zhu, Y., Mu, L., 2021. Planktic foraminifera of the upper Barremian–Aptian black shale intervals from the Chaqiela section (Gamba, southern Tibet): Biostratigraphic and palaeoenvironmental implications. Cretac. Res. 127, 104934.
Fu, X., Wang, J., Zeng, S., Feng, X., Wang, D., Song, C., 2017. Continental weathering and palaeoclimatic changes through the onset of the Early Toarcian oceanic anoxic event in the Qiangtang Basin, eastern Tethys. Palaeogeogr. Palaeoclimatol. Palaeoecol. 487, 241–250.
Gale, A.S., Bown, P., Caron, M., Crampton, J., Crowhurst, S.J., Kennedy, W.J., Petrizzo, M.R., Wray, D.S., 2011. The uppermost Middle and Upper Albian succession at the Col de Palluel, Hautes-Alpes, France: an integrated study (ammonites, inoceramid bivalves, planktonic foraminifera, nannofossils, geochemistry, stable oxygen and carbon isotopes, cyclostratigraphy). Cretac. Res. 32, 59–130.
Gambacorta, G., Jenkyns, H.C., Russo, F., Tsikos, H., Wilson, P.A., Faucher, G., Erba, E., 2015. Carbon-and oxygen-isotope records of mid-Cretaceous Tethyan pelagic sequences from the Umbria– Marche and Belluno Basins (Italy). Newsl. Stratigr. 48, 299–323.
Giraud, F., Olivero, D., Baudin, F., Reboulet, S., Pittet, B., Proux, O., 2003. Minor changes in surfacewater fertility across the oceanic anoxic event 1d (latest Albian, SE France) evidenced by calcareous nannofossils. Int. J. Earth Sci. 92, 267–284.
Gradstein, F.M., Ogg, J.G., Smith, A.G., 2004. A geologic Time Scale 2004. Cambridge University Press, Cambridge, UK, p. 589.
Grocke, D.R., Ludvigson, G.A., Witzke, B.L., Robinson, S.A., Joeckel, R.M., Ufnar, D.F., Ravn, R.L., 2006. Recognizing the Albian-Cenomanian (OAE1d) sequence boundary using plant carbon isotopes: Dakota Formation, Western Interior Basin, USA. Geology 34, 193–196.
Hammer, Ø., Harper, D.A.T., Ryan, P.D., 2001. PAST: palaeontological Statistics software package for education and data analysis. Palaeontol. Electron. 4, 1.
Herrle, J.O., 2003. Reconstructing nutricline dynamics of mid-cretaceous oceans: evidence from calcareous nannofossils from the Niveau Paquier black shale (SE France). Mar. Micropaleontol. 47, 307–321.
Herrle, J.O., Mutterlose, J., 2003. Calcareous nannofossils from the Aptian-Lower Albian of southeast France: palaeoecological and biostratigraphic implications. Cretac. Res. 24, 1–22.
Herrle, J.O., Pross, J., Friedrich, O., Kößler, P., Hemleben, C., 2003. Forcing mechanisms for mid-Cretaceous black shale formation: evidence from the Upper Aptian and Lower Albian of the Vocontian Basin (SE France). Palaeogeogr. Palaeoclimatol. Palaeoecol. 190, 399–426.
Hesselbo, S.P., Grocke, D.R., Jenkyns, H.C., Bjerrum, C.J., Farrimond, P., Bell, H.S.M., Green, O.R., 2000. Massive dissociation of gas hydrate during a Jurassic oceanic anoxic event. Nature 406, 392–395.
Hoshina, K., Wang, Y., Jiang, S., Lozar, F., Persico, D., Villa, G., Jordan, R.W., 2021. Eocene calcareous nannofossils from southern Tibet: paleoceanographic implications for the closure of the eastern Tethys Ocean. Mar. Micropaleontol. 167, 102031.
Hu, X., Jansa, L., Wang, C., 2008. Upper Jurassic–Lower Cretaceous stratigraphy in south-eastern Tibet: a comparison with the western Himalayas. Cretac. Res. 29, 301–315.
Hu, X., Li, J., An, W., Wang, J., 2017. The redefinition of Cretaceous–Paleogene lithostratigraphic units and tectonostratigraphic division in southern Tibet. Earth Sci. Front. 24, 174–194.
Jenkyns, H.C., 2010. Geochemistry of oceanic anoxic events. Geochem. Geophys. Geosyst. 11, Q03004.
Jiang, S., Zhang, A., 2016. A slide-making technique for preparing calcareous nannofossils from large amount of samples. Acta Micropalaeontol. Sin. 33, 207–210 (In Chinese with English abstract).
Kabanov, P., Hauck, T.E., Gouwy, S.A., Grasby, S.E., van der Boon, A., 2023. Oceanic anoxic events, photic-zone euxinia, and controversy of sea-level fluctuations during the Middle-Late Devonian. Earth Sci. Rev. 241, 104415.
Kennedy, W.J., Gale, A.S., Bown, P.R., Caron, M., Davey, R.J., Grocke, J., Wray, D.S., 2000. Integrated stratigraphy across the Aptian-Albian boundary in the Marnes Bleues, at the Col de Pre-Guittard, Arnayon Drome, and at Tartonne (Alpes-de-Haute-Provence), France: a candidate Global Boundary Stratotype Section and boundary point for the base of the Albian Stage. Cretac. Res. 21, 591–720.
Li, X., Wang, C., Hu, X., 2005. Stratigraphy of deep-water Cretaceous deposits in Gyangze, southern Tibet, China. Cretac. Res. 26, 33–41.
Li, J., Peng, J., Zhang, Q., 2016. Palynological assemblages from the Cretaceous succession at Chaqiela, Gamba county, Xizang. Acta Palaeontol. Sin. 55, 346–366.
Li, X., Hu, X., An, W., Liu, Q., Garzanti, E., Meng, J., 2022. From Neo-Tethyan convergence to India-Asia collision: radiolarian biostratigraphy of the Cretaceous to Paleocene deep-water Tethys Himalaya. Newslett. Stratigr. 56, 33–52.
Liu, G., Einsele, G., 1994. Sedimentary history of the Tethyan basin in the Tibetan Himalayas. Geol. Rundsch. 83, 32–61.
Mutterlose, J., Bornemann, A., Herrle, J., 2005. Mesozoic calcareous nannofossils — state of the art. Paläontol. Z. 79, 113–133.
Perch-Nielsen, K., 1985. Mesozoic calcareous nannofossils. In: Bolli, H.M., Saunders, J.B., Perch-Nielsen, K. (Eds.), Plankton Stratigraphy: Volume 1, Planktic Foraminifera, Calcareous Nannofossils and Calpionellids. Cambridge University Press, pp. 329–426.
Ratschbacher, L., Frisch, W., Liu, G., Chen, C., 1994. Distributed deformation in southern and western Tibet during and after the India- Asia collision. J. Geophys. Res. Solid Earth 99, 19917–19945.
Reershemius, T., Planavsky, N.J., 2021. What controls the duration and intensity of ocean anoxic events in the Paleozoic and the Mesozoic? Earth Sci. Rev. 221, 103787.
Richey, J.D., Upchurch, G.R., Montañez, I.P., Lomax, B.H., Suarez, M.B., Crout, N.M.J., Joeckel, R.M., Ludvigson, G.A., Smith, J.J., 2018. Changes in CO2 during Ocean Anoxic Event 1d indicate similarities to other carbon cycle perturbations. Earth Planet. Sci. Lett. 491, 172–182.
Robinson, S.A., Clarke, L.J., Nederbragt, A., Wood, I.G., 2008. Mid-Cretaceous oceanic anoxic events in the Pacific Ocean revealed by carbon-isotope stratigraphy of the Calera Limestone, California, USA. Geol. Soc. Am. Bull. 120, 1416–1427.
Roth, P.H., 1978. Cretaceous nannoplankton biostratigraphy and oceanography of the northwestern Atlantic Ocean. Initial Rep. Deep Sea Drill. Proj. 44, 731–759.
Roth, P.H., Bowdler, J.L., 1981. Middle Cretaceous calcareous nannoplankton biostratigraphy and oceanography of the Atlantic Ocean. In: Warme, J.E., Douglas, R.G., Winterer, E.L. (Eds.), The Deep Sea Drilling Project: A Decade of Progress. Special Publication - Society of Economic Paleontologists and Mineralogists, Houston, TX (USA), pp. 517–546, 4 Apr 1979.
Roth, P.H., Krumbach, K.R., 1986. Middle Cretaceous calcareous nannofossil biogeography and preservation in the Atlantic and Indian oceans: Implications for paleoceanography. Mar. Micropaleontol. 10, 235–266.
Schlanger, S.O., Jenkyns, H.C., 1976. Cretaceous oceanic anoxic events: causes and consequences. Geol. Mijnb. 55, 179–184.
Svabenicka, L., Li, X.H., Jansa, L.F., Wei, Y.S., 2010. Nannofossil biostratigraphy of the Lower Cretaceous Shadui Formation (Northern Tethyan Himalayas, Southern Tibet). Geol. Carpath. 61, 383–391.
Tapponnier, P., Mercier, J.L., Proust, F., Andrieux, J., Armijo, R., Bassoullet, J.P., Brunel, M., Burg, J.P., Colchen, M., Dupré, B., Girardeau, J., Marcoux, J., Mascle, G., Matte, P., Nicolas, A., Tingdong, L., Xuchang, X., Chenfa, C., Paoyu, L., Guangcen, L., Naiwen, W., Guoming, C., Tonglin, H., Xibin, W., Wanming, D., Haixiang, Z., Huaibin, S., Yongong, C., Ji, Z., Hongrong, Q., 1981. The Tibetan side of the India–Eurasia collision. Nature 294, 405–410.
Them, T.R., Gill, B.C., Selby, D., Gröcke, D.R., Friedman, R.M., Owens, J.D., 2017. Evidence for rapid weathering response to climatic warming during the Toarcian Oceanic Anoxic Event. Sci. Rep. 7, 5003.
Thierstein, H.R., Roth, P.H., 1991. Stable isotopic and carbonate cyclicity in Lower Cretaceous deep-sea sediments: dominance of diagenetic effects. Mar. Geol. 97, 1–34.
Tiraboschi, D., Erba, E., Jenkyns, H.C., 2009. Origin of rhythmic Albian black shales (Piobbico core, Central Italy): calcareous nannofossil quantitative and statistical analyses and paleoceanographic reconstructions. Paleoceanography 24.
Tremolada, F., Erba, E., Bralower, T.J., 2006. Late Barremian to early Aptian calcareous nannofossil paleoceanography and paleoecology from the Ocean Drilling Program Hole 641C (Galicia Margin). Cretac. Res. 27, 887–897.
Wagreich, M., Hu, X.M., Sageman, B., 2011. Causes of oxic-anoxic changes in Cretaceous marine environments and their implications for Earth systems-An introduction. Sediment. Geol. 235, 1–4.
Wan, X., 1985. The Cretaceous Stratigraphy and Foraminiferal Fauna of the Gangba Area, Tibet. Qinghai-Tibet Plateau Geol. Collect. 203–227 (in Chinese with English abstract).

Wan, X., Zhao, W., Li, G., 2000. Rrestudy of the Upper Cretaceous in Gamba, Tibet. Geoscience 281–285 (in Chinese with English abstract).
Wan, X., Wignall, P.B., Zhao, W., 2003. The Cenomanian–Turonian extinction and oceanic anoxic event: evidence from southern Tibet. Palaeogeogr. Palaeoclimatol. Palaeoecol. 199, 283–298.
Wang, Y., Sun, D., He, G., 1980. New insights into the stratigraphic research in the Himalayan region (within China). J. Stratigr. 4, 55–59.
Wang, C., Xia, D., Zhou, X., Chen, J., Lu, Y., Wang, G., He, Z., Li, X., Wan, X., Zeng, Q., Pubu, C., Liu, Z., 1996. Field Trip Guide T121/T387, Geology between the Indus-Yarlung Zangbo Suture Zone and the Himalaya Mountains, Xizang (Tibet). Geological Publishing House, Beijing, China, p. 72.
Wang, C.S., Hu, X.M., Sarti, M., Scott, R.W., Li, X.H., 2005. Upper Cretaceous oceanic red beds in southern Tibet: a major change from anoxic to oxic, deep-sea environments. Cretac. Res. 26, 21–32.
Wang, Y., Jiang, S., Hu, X., Li, J., Kulhanek, D.K., Pospichal, J.J., Watkins, D.K., 2022. Lower Cretaceous calcareous nannofossils and their biostratigraphic and paleoceanographic implications in Southern Tibet. Mar. Micropaleontol. 175, 102159.
Watkins, D.K., 1992. Upper cretaceous nannofossils from Leg 120, Kerguelen plateau, southern ocean. In: Wise Jr., S.W., Schlich, R., et al. (Eds.), Proceedings of the Ocean Drilling Program, Scientific Results. Ocean Drilling Program, College Station, TX.
Watkins, D.K., Bergen, J.A., 2003. Late Albian adaptive radiation in the Calcareous Nannofossil Genus Eiffellithus. Micropaleontology 49, 231–251.
Watkins, D.K., Cooper, M.J., Wilson, P.A., 2005. Calcareous nannoplankton response to late Albian oceanic anoxic event 1d in the western North Atlantic. Paleoceanography 20.
Wen, S., 1974. The Cretaceous and Tertiary System. A Report of the Scientific Expedition in the Mount Qomolangma Region (1966–1968). Science Press, Beijing (in Chinese with English abstract).
Willems, H., Zhou, Z., Zhang, B., Gräfe, K.-U., 1996. Stratigraphy of the upper cretaceous and lower tertiary strata in the Tethyan Himalayas of Tibet (Tingri area, China). Geol. Rundsch. 85, 723–754.
Williams, J.R., Bralower, T.J., 1995. Nannofossil assemblages, fine fraction stable isotopes, and the paleoceanography of the Valanginian-Barremian (Early Cretaceous) North Sea Basin. Paleoceanography 10, 815–839.
Wilson, P.A., Norris, R.D., 2001. Warm tropical ocean surface and global anoxia during the mid-cretaceous period. Nature 412, 425–429.
Wise, S.W., 1988. Mesozoic-cenozoic history of calcareous nannofossils in the region of the southern ocean. Palaeogeogr. Palaeoclimatol. Palaeoecol. 67, 157–179.
Xu, Y.-L., Mao, S.-Z., 1992. Cretaceous-Early Tertiary calcareous nannofossils from southern Xizang (Tibet) and their sedimentary environment. Acta Micropalaeontol. Sin. 9, 331–347.
Yao, H., Chen, X., Melinte-Dobrinescu, M.C., Wu, H., Liang, H., Weissert, H., 2018. Biostratigraphy, carbon isotopes and cyclostratigraphy of the Albian-Cenomanian transition and Oceanic Anoxic Event 1d in southern Tibet. Palaeogeogr. Palaeoclimatol. Palaeoecol. 499, 45–55.
Yao, H., Chen, X., Yin, R., Grasby, S.E., Weissert, H., Gu, X., Wang, C., 2021. Mercury evidence of intense volcanism preceded Oceanic Anoxic Event 1d. Geophys. Res. Lett. 48, e2020GL091508.
Yin, A., Harrison, T.M., 2000. Geologic evolution of the Himalayan-Tibetan Orogen. Annu. Rev. Earth Planet. Sci. 28, 211–280.
Young, J.R., Bown, P.R., Lees, J.A., 2017. Nannotax3 Website. Int. Nannoplankton Assoc. http://www.mikrotax.org/Nannotax3.
Zhang, Q., Willems, H., Ding, L., Gräfe, K.-U., Appel, E., 2012. Initial India-Asia Continental Collision and Foreland Basin Evolution in the Tethyan Himalaya of Tibet: evidence from Stratigraphy and Paleontology. J. Geol. 120, 175–189.
Zhang, X., Chen, K., Hu, D., Sha, J., 2016. Mid-Cretaceous carbon cycle perturbations and Oceanic Anoxic Events recorded in southern Tibet. Sci. Rep. 6, 39643.
Zhang, Y., Liu, X., Watkins, D.K., Bruno, M.D.R., Yao, H., Han, K., Guo, H., Zhu, S., Chen, X., 2023. The Cretaceous (early Albian to early Campanian) biostratigraphy and palaeotemperature reconstruction of the eastern Tethys: Calcareous nannofossil evidence from southern Tibet, China. Palaeogeogr. Palaeoclimatol. Palaeoecol. 613, 111417.
Zhong, S., Zhou, Z., Willems, H., Zhang, B., Zhu, Y., 2000. The middle Cretaceous calcareous nannofossil zones in Gamba area, southern Xizang (Tibet), China and the Cenomanian-Turonian boundary. Acta Palaeontol. Sin. 39, 313–325.